Very Wideband Operation of Twin-layer Inset Dielectric Guide

Steve R. Pennock, *Member, IEEE,* Narian Izzat and Tullio Rozzi, *Fellow, IEEE*

Abstract—**Inset Dielectric Guide has been proposed as a transmission line for millimeter wave circuits and antennas. However, little has been determined concerning the guide parameters which control the bandwidth of the guide or the achievable bandwidth limits. In order to investigate these parameters we have analyzed the IDG structure in the case where the dielectric filling may be a multilayer structure. As a result, we have found that while IDG with a single filling can have a bandwidth exceeding that of rectangular metal waveguide, the use of just two dielectric layers can give bandwidths exceeding those typical of double ridge waveguide.**

I. Introduction

INSET DIELECTRIC GUIDE (IDG), illustrated in Fig. 1, has shown promise as a low loss transmission line for microwave and millimetric applications. It is a very attractive circuit medium in comparison to dielectric guides such as image line or insular line in view of its ability to negotiate bends with minimal loss [1]. Further, the fabrication difficulties encountered with Image or Insular guide are eased, and low cost lightweight circuits could be realized using plastic moulding and spray metallization techniques.

Dipole Array antennas are very simple to construct in IDG, and have shown good input match and low cross polarization [2]–[4] in both deep slot and shallow slot configurations. These configurations allow both horizontal and vertical polarization antennas to be designed in IDG. The antennas have a flat radiating surface, which combined with the possibilities of lightweight construction make IDG antennas appear very suited to avionic applications.

The properties of parallel coupled lines in IDG have recently been investigated [5], showing good predictability and performance. It is therefore now possible to consider the construction of directional couplers and bandpass filters in IDG, and thereby include basic filtering and power splitting operations in the same IDG circuit media as the antenna.

The influence of aspect ratio and dielectric filling on the mode spectrum, and hence the monomode bandwidth, of IDG has received little or no attention in the past. In this paper we consider the control we can exert over the monomode bandwidth through using different dielectrics and combinations of dielectrics in the IDG slot. The combinations considered here are of dielectrics layered as shown in Fig. 2. Consequently, we analyze the structure using a Transverse Resonance Diffraction [6]–[8] analysis cast in the direction through the layers.

It appears that, by the use of an IDG filling with just two layers, monomode bandwidths larger than that of double ridge waveguide can be easily achieved.

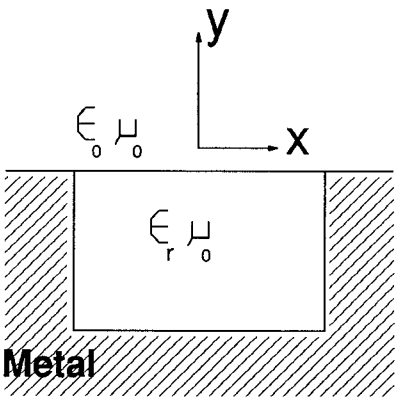

Fig. 1. Cross section of Inset Dielectric Guide.

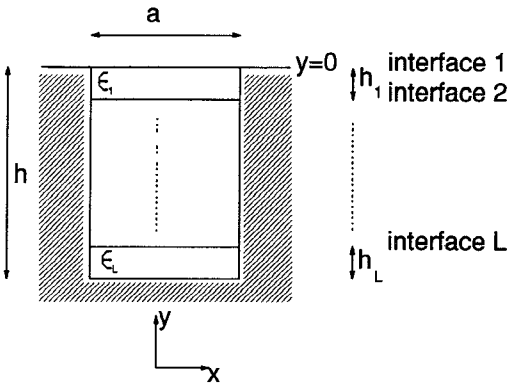

Fig. 2. Cross section of multilayered Inset Dielectric Guide.

II. Theory

Fig. 2 gives the cross section of a multilayered IDG structure. The full six component hybrid field in the air region and each of the dielectric layers can be expressed as the superposition of TM-to-y (e-mode) and TE-to-y

Manuscript received August 22, 1991; revised March 12, 1992.

S. R. Pennock is with the School of Electronic and Electrical Engineering, University of Bath, Claverton Down, Bath, BA2 7AY, England.

N. Izzat and T. Rozzi are with the Dipartmento di Electronica e Automatica, Universita degli Studi di Ancona, 60131 Ancona, Italy.

IEEE Log Number 9202134.

(h-mode) fields. These can in turn be derived from y-directed electric and magnetic Hertzian potential functions respectively [9].

The total fields may be explicitly written from the Hertzian potentials:

$$\underline{\Pi}_h = \hat{y}\Psi_h(x, y)e^{-j\beta z} \quad \underline{\Pi}_e = \hat{y}\Psi_e(x, y)e^{-j\beta z} \tag{1}$$

using

$$\underline{E} = -j\omega\mu_0\nabla \times \underline{\Pi}_h + \epsilon_r K_0^2 \underline{\Pi}_e + \nabla\nabla \cdot \underline{\Pi}_e$$

$$\underline{H} = -j\omega\epsilon_0\epsilon_r\nabla \times \underline{\Pi}_e + \epsilon_r K_0^2 \underline{\Pi}_h + \nabla\nabla \cdot \underline{\Pi}_h \tag{2}$$

where β is the phase constant of the mode. The boundary conditions to be obeyed at $y = 0$ are as follows:

$$E_{x,z}(x, 0^+) = E_{x,z}(x, 0^-) = E_{x,z}(x, 0) \tag{3a}$$

$$H_{x,z}(x, 0^+) = H_{x,z}(x, 0^-) \qquad |x| < a/2 \tag{3b}$$

Considering the air region and the uppermost dielectric layer, the following potential functions are chosen for the two regions:

In the dielectric layer, $0 < y < h_1$ we have:

$$\Psi_e(x, y) = \sum_n^{\infty} \frac{I'_{1n}}{j\omega\epsilon_1} \frac{1}{\sqrt{((n\pi/a)^2 + \beta^2)}} \phi_{en}(x) \frac{jY'_1(n) \sin k_{1n}(y + h_1) + Y'^D_2(n) \cos k_{1n}(y + h_1)}{jY'_1(n) \sin k_{1n}h_1 + Y'^D_2(n) \cos k_{1n}h_1} \tag{4a}$$

$$\Psi_h(x, y) = \sum_n^{\infty} \frac{V''_{1n}}{j\omega\mu_0} \frac{1}{\sqrt{((n\pi/a)^2 + \beta^2)}} \phi_{hn}(x) \frac{Y''_1(n) \cos k_{1n}(y + h_1) + jY''^D_2(n) \sin k_{1n}(y + h_1)}{Y''_1(n) \cos k_{1n}h_1 + jY''^D_2(n) \sin k_{1n}h_1} \tag{4b}$$

while in the air region, $y > 0$

$$\Psi_e(x, y) = \int_0^{\infty} \frac{I'(\rho)}{j\omega\epsilon_0} \frac{1}{\sqrt{\rho^2 + \beta^2}} \phi_e(\rho, x)e^{-jk_y(\rho)y}\, d\rho \tag{5a}$$

$$\Psi_h(x, y) = \int_0^{\infty} \frac{V''(\rho)}{j\omega\mu_0} \frac{1}{\sqrt{\rho^2 + \beta^2}} \phi_h(\rho, x)e^{-jk_y(\rho)y}\, d\rho. \tag{5b}$$

The y-directed wavenumber for the slot region is given by

$$k_{in}^2 = \epsilon_{ir}K_0^2 - \left(\frac{n\pi}{a}\right)^2 - \beta^2 \tag{6a}$$

and in the air region continuum by

$$k_y(\rho)^2 = K_0^2 - \rho^2 - \beta^2 \tag{6b}$$

Y'_i, Y''_i denote the characteristic admittances for the e and h-modes, respectively, and Y'^D_2, Y''^D_2 denote the respective e-mode and h-mode input admittances looking down at interface 2.

For modes with even-E_z symmetry suitable forms for the x-dependence of the potential functions are

$$\phi_{hn}(x) = \frac{2}{\sqrt{a}} \sin(n\pi/a)x \quad \phi_{en}(x) = \frac{2}{\sqrt{a}} \cos(n\pi/a)x \qquad (n = 1, 3) \tag{7}$$

$$\phi_h(x, \rho) = \frac{2}{\sqrt{\pi}} \sin \rho x \quad \phi_e(x, \rho) = \frac{2}{\sqrt{\pi}} \cos \rho x \qquad (\rho > 0). \tag{8}$$

For the odd-E_z symmetry modes we simply exchange sine and cosine functions. The general expression for the input admittances looking down at interface i in the slot is given by

$$Y_i^D(n) = Y_i(n) \frac{jY_i(n) \tan k_{in}h_i + Y^D_{i-1}(n)}{jY^D_{i-1}(n) \tan k_{in}h_i + Y_i(n)}. \tag{9}$$

The input admittances looking at Lth interface are

$$Y_L'^D(n) = \frac{\omega\epsilon_0\epsilon_{Lr}}{k_{Ln}} \frac{1}{j \tan k_{Ln}h_L} \tag{10a}$$

$$Y_L''^D(n) = \frac{k_{Ln}}{\omega\mu_0} \frac{1}{j \tan k_{Ln}h_L}. \tag{10b}$$

In order to enforce the boundary conditions (3b), the tangential magnetic fields at the interface are first expressed as a function of the tangential electric fields [10] to give

$$\begin{bmatrix} \tilde{y}_{11} & \tilde{y}_{12} \\ \tilde{y}_{21} & \tilde{y}_{22} \end{bmatrix} \begin{bmatrix} E_x(x, 0) \\ E_z(x, 0) \end{bmatrix} = \underline{0} \tag{11a}$$

It has been previously noted that integrating by parts improves convergence [10]. Thus integrating (11a) by parts, gives

$$\begin{bmatrix} \tilde{Y}_{11} & \tilde{Y}_{12} \\ \tilde{Y}_{21} & \tilde{Y}_{22} \end{bmatrix} \begin{bmatrix} E_x(x, 0) \\ \partial_x E_z(x, 0) \end{bmatrix} = \underline{0} \tag{11b}$$

where $\tilde{Y}_{ij}$ are admittance operators which are given in Appendix A.

The dispersion relation (11b) can be solved by applying the Galerkin procedure. $E_x(x, 0)$, $\partial_x E_z(x, 0)$ are expressed in terms of a complete set of basis functions:

$$E_x(x, 0) = \sum_{i=0}^{\infty} X_i E_{xi}(x) \quad \partial_x E_z(x, 0) = \sum_{i=0}^{\infty} Z_i E'_{zi}(x). \tag{12}$$

In order to obtain rapid convergence to the solution of the dispersion relation, the following weight function is introduced into the basis functions [10]:

$$W(2x/a) = (1 - (2x/a)^2)^{-1/3}. \tag{13}$$

A choice of functions that are orthogonal to the weight function (13) are the Gegenbauer polynomials [8], $C_n^{\nu}(2x/a)$ with $\nu = \frac{1}{6}$.

As a result, both $E_x(x, 0)$ and $\delta_x E_z(x, 0)$ can both be represented in terms of the same set of basis functions to give:

$$E_{xi} = E'_{zi} = f_i(x) = \frac{c_i^{\nu}(2x/a)}{(1 - (2x/a)^2)^{-1/3}} \qquad |x| < a/2. \tag{14}$$

The Galerkin procedure is completed by taking the inner product of the basis functions with (11b), resulting in the determinant equation:

$$\begin{bmatrix} \langle E_{xi}\tilde{Y}_{11ij}E_{xj}\rangle & \langle E_{xi}\tilde{Y}_{12ij}E'_{zj}\rangle \\ \langle E'_{zi}\tilde{Y}_{21ij}E_{xj}\rangle & \langle E'_{zi}\tilde{Y}_{22ij}E'_{zj}\rangle \end{bmatrix} \begin{bmatrix} \underline{X} \\ \underline{Z} \end{bmatrix} = 0. \quad (15)$$

A search for the zeros of the determinant then gives the solutions for the required propagation coefficients.

III. Results

A. Convergence of Solutions

The convergence of solutions for the fundamental mode, as a function of the number of basis functions, for a multilayered IDG is given in Table I. It can be seen from the table that convergence to 3 significant figures is achieved using just two sets of basis functions for each of the tangential electric field components at the slot-air interface.

TABLE I
CONVERGENCE OF SOLUTIONS FOR FUNDAMENTAL MODE OF IDG WITH TWO DIELECTRIC LAYERS IN THE SLOT. A 2 × 2 BASIS SET GENERALLY GIVES NO MORE THAN 0.25% ERROR. (GUIDE PARAMETERS ARE a = 1.016 cm, h = 1.524 cm, h_2 = 1.46 cm, ϵ_{r1} = 10.2, ϵ_{r2} = 2.04.)

	β/k_0 As a Function of the Number of Basis Functions		
Frequency (GHz)	1 × 1 Basis	2 × 2 Basis	3 × 3 Basis
4	1.0947	1.0701	1.0686
6	1.3213	1.2930	1.2913
8	1.4274	1.3939	1.3913
10	1.5010	1.4569	1.4544
12	1.5746	1.5068	1.5034

B. Comparison with Measured Results

Experiments were carried out for a number of different cross sections of IDG in order to assess the accuracy of the analysis presented in the previous sections.

The experiment was performed using the resonant section technique. A section of IDG is terminated with short circuit plates at both ends. Energy was then coupled into the IDG section by inserting small magnetic loop probes through the short circuit plates resulting in a weak coupling mechanism. Thus the section would be virtually short-circuited at both ends, and would only support standing waves that have "zero" E_x, E_y fields at each end. Consequently energy only significantly couples into the section at specific resonant frequencies were the line section is an integral numbers of half wavelengths long. The transmission response over a range of frequencies was obtained using a HP8510B analyzer, and weak coupling is maintained by ensuring that the peak transmission at the resonant point was always less than −25 dB. The transmission peaks are very sharp, thereby allowing the resonant frequencies to be measured accurately.

The parity of the excited fields can be controlled by changing the orientation of the magnetic probes. In the parity convention used here we describe the parity of the E_z field. For odd parity modes H_x is zero at the center of the IDG line while H_y is finite. Therefore a vertically orientated probe positioned at the line center will only excite even parity modes. Similarly, for even parity modes H_y is zero at the guide center, H_x is finite, and a horizontally orientated magnetic probes excites only odd parity modes. An example of the insertion loss of a resonant section of IDG for horizontal and vertical orientation of the magnetic probes is shown in Fig. 3. This clearly illustrates the ability to excite even and odd parity modes independently using this technique, and so independently measure the fundamental and first higher order modes of our IDG lines.

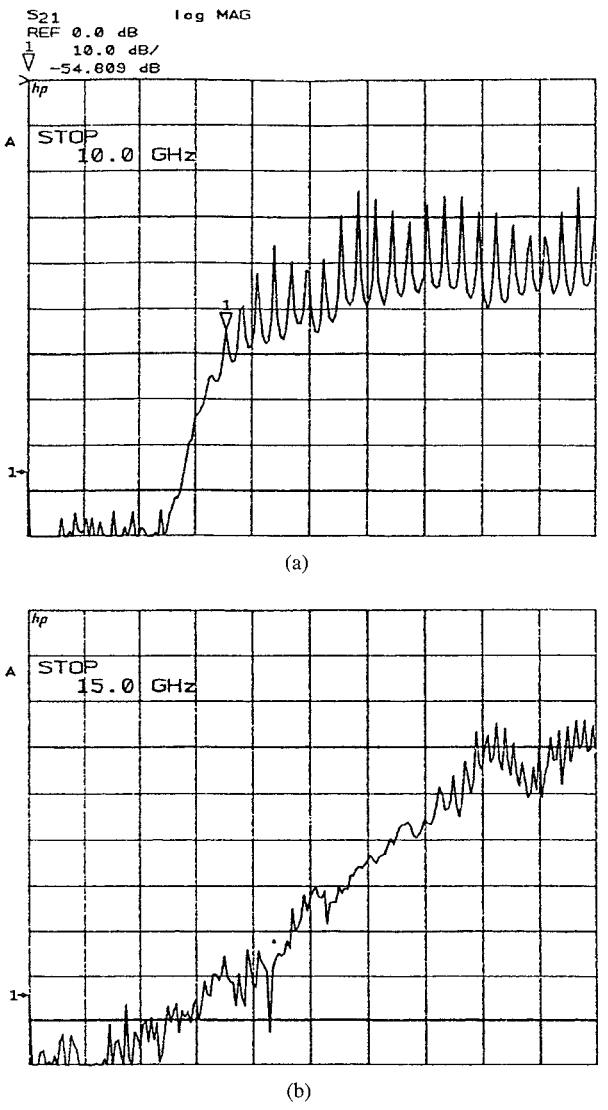

(a)

(b)

Fig. 3. Measured Insertion loss of a resonant section of two-layer IDG with slot dimensions are a = 1.016 cm, h = 1.524 cm. The upper layer is 0.635 mm thick and has ϵ_r = 10.2, while the lower layer is PTFE where ϵ_r = 2.04. Insertion loss is shown in the range −100 dB to 0 dB. The measurements are for (a) the fundamental (odd parity) mode, 45 MHz–10 GHz, (b) the first higher order (even parity) mode, 45 MHz–15 GHz.

A comparison of theoretical and experimental results obtained for two sample geometries are shown in Figures 4 and 5. Clearly there is very good agreement between

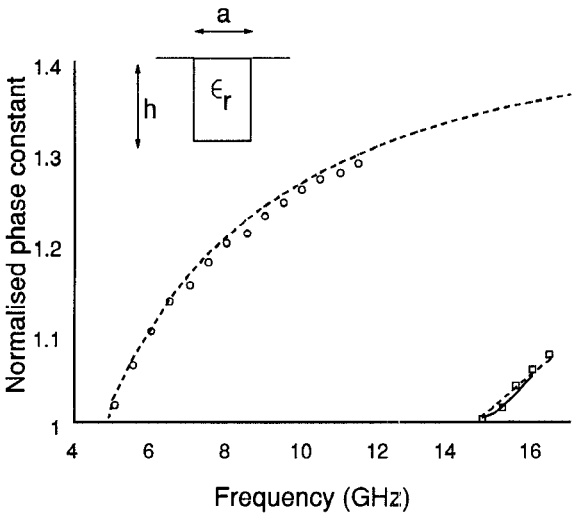

Fig. 4. Dispersion data for single layer PTFE filled IDG with optimum aspect ratio for maximum monomode bandwidth, [a] = 1.016 cm, h = 1.524 cm. Normalized phase constant (β/k_0) is shown as a function of frequency. Theoretical data for even parity (———) and odd parity (– – –) compares well with experimental even parity (□) and odd parity (○) points.

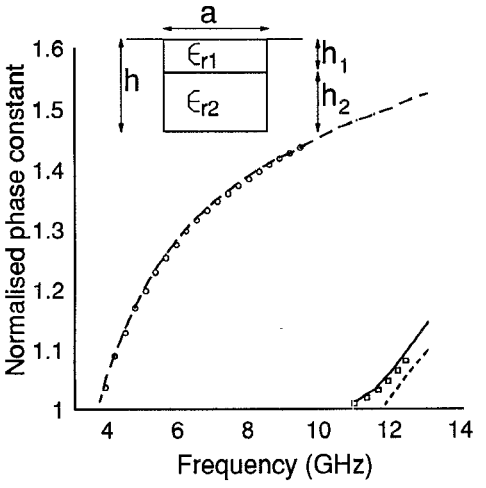

Fig. 5. Normalized phase constant (β/k_0) dispersion data for the two-layer IDG examined in Fig. 3. Theoretical curves (even parity ———, odd parity – – –) compare well with the experimental points (even parity □, odd parity ○).

experiment and theory for both fundamental and first higher order modes.

IV. Bandwidth Control in Single-Layered IDG

In Fig. 6 (a)–(d), dispersion curves are presented for the first two modes in a single-layered IDG keeping the slot depth, h, fixed and varying a, the slot aperture. In order to provide a measure of the useful bandwidth of the guide as the aspect ratio (a/h) is varied, we define the monomode bandwidth in terms of the cut-off frequencies of the fundamental and first higher order modes, f_0 and f_1, respectively:

$$\text{monomode bandwidth} = \frac{f_1 - f_0}{f_1 + f_0} \times 100\% \qquad (16)$$

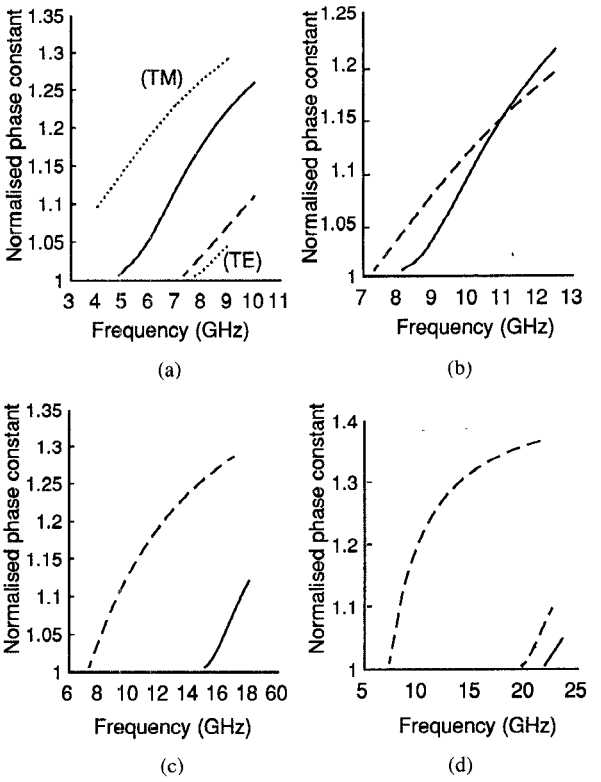

Fig. 6. Normalized phase constant (β/k_0) dispersion data for single layer PTFE filled IDG for both even parity (———) and odd parity (– – –) modes. The slot depth is fixed at h = 1.524 cm while slot widths of (a) a = 4 cm, (b) a = 2 cm, (c) a = 1 cm, and (d) a = 0.6 cm are considered. The modes of a grounded slab of thickness h = 1.524 cm are also shown in (a) for comparison.

where the monomode bandwidth is expressed as a percentage. It is worth bearing in mind for comparison purposes that, in this definition, a 2:1 aspect ratio rectangular waveguide has a monomode bandwidth of 33% but it is generally used over only a 20% bandwidth.

As the aspect ratio is increased, the behavior of the guide is expected to approach that of a grounded dielectric slab of thickness equal to h, the slot depth. In Fig. 6(a) the first two modes of such a dielectric slab are also included for comparison with the dispersion curves of an IDG with a relatively large aspect ratio. As the aspect ratio increases the monomode bandwidth would tend towards that of the dielectric slab, i.e., 100% as the slab has no cut-off for the fundamental mode. Although a large monomode bandwidth is achievable by increasing the aspect ratio, this is not considered to be of practical use since the increase in aspect ratio will result in a lack of lateral field confinement. This field confinement is one of the main advantages of IDG.

Decreasing the IDG aspect ratio produces an increase in the cutoff frequency of the fundamental even mode until an aspect ratio of about 2 is reached (Fig. 6(b)). At this point the first even mode and the first odd mode propagate at nearly equal phase velocities. Below an aspect ratio of 2, the fundamental mode becomes odd in parity. Thus at an aspect ratio of around 2, the monomode bandwidth drops down to 0%, and begins to increase again as the aspect ratio is further decreased. This is shown in Fig.

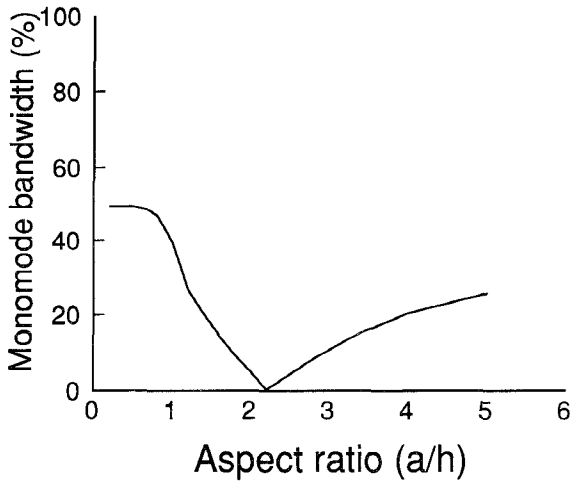

Fig. 7. Monomode bandwidth of single layer PTFE filled IDG as a function of aspect ratio (a/h) where the slot depth, h, is fixed and slot width, a, is varied.

6(c) and (d). At an aspect ratio of 0.6, the cutoff frequency of the second odd mode becomes even higher than that of the first even mode.

By comparing the Fig. 6(a)–(d), it can be seen that the cutoff of the odd parity mode is not greatly affected by the change in aperture. However, the cutoff of the even parity mode increases rapidly as the side walls are brought in. A possible explanation for this behavior might be seen if the original TM and TE modes of the slab waveguide (IDG with side walls removed to infinity) are considered. The TM-to-y mode has H_x, E_y, E_z field components, while the TE-to-y mode has E_x, H_y, H_z components. Bringing in the side walls in the slot introduces singular behavior in some of the field components. In addition however, the three TM components are forced to zero at the side walls, whereas the TE components do not have this boundary condition imposed upon them. Thus it can be argued that the TM mode is perturbed strongly by the presence of the conducting walls, and its cutoff frequency increases as the width of the slot decreases.

Fig. 6(a)–(d) reveal an important mechanism of bandwidth control. The relative cutoff between odd parity modes and even parity modes can be controlled through changing the width of the slot aperture.

Fig. 7, gives a plot of monomode bandwidth versus aspect ratio while the slot depth, h, is kept fixed. From the figure it can be seen that in a deep slot the bandwidth maximizes at 49% at an aspect ratio of 0.66. As such, this is significantly greater than the maximum 33% obtainable in rectangular waveguide. It is noted that below this aspect ratio the first higher order mode is also of odd parity (see Fig. 6(d)) and thus the control mechanism mentioned above is no longer of any use below an aspect ratio of 0.67.

The magnitude of the E_x field component over the cross section of the guide is plotted in Fig. 8 for the three modes of Fig. 6(d) at 22 GHz. The three plots illustrate the singular nature of the fields at the metal corners of the IDG cross section. They also indicate the nature of higher order modes and hence the cross section parameter that primarily controls their cut-off. The first higher order mode is higher in order than the fundamental mode in its dependence down into the slot. The second higher order mode has a field pattern which is higher in order in its dependence across the slot.

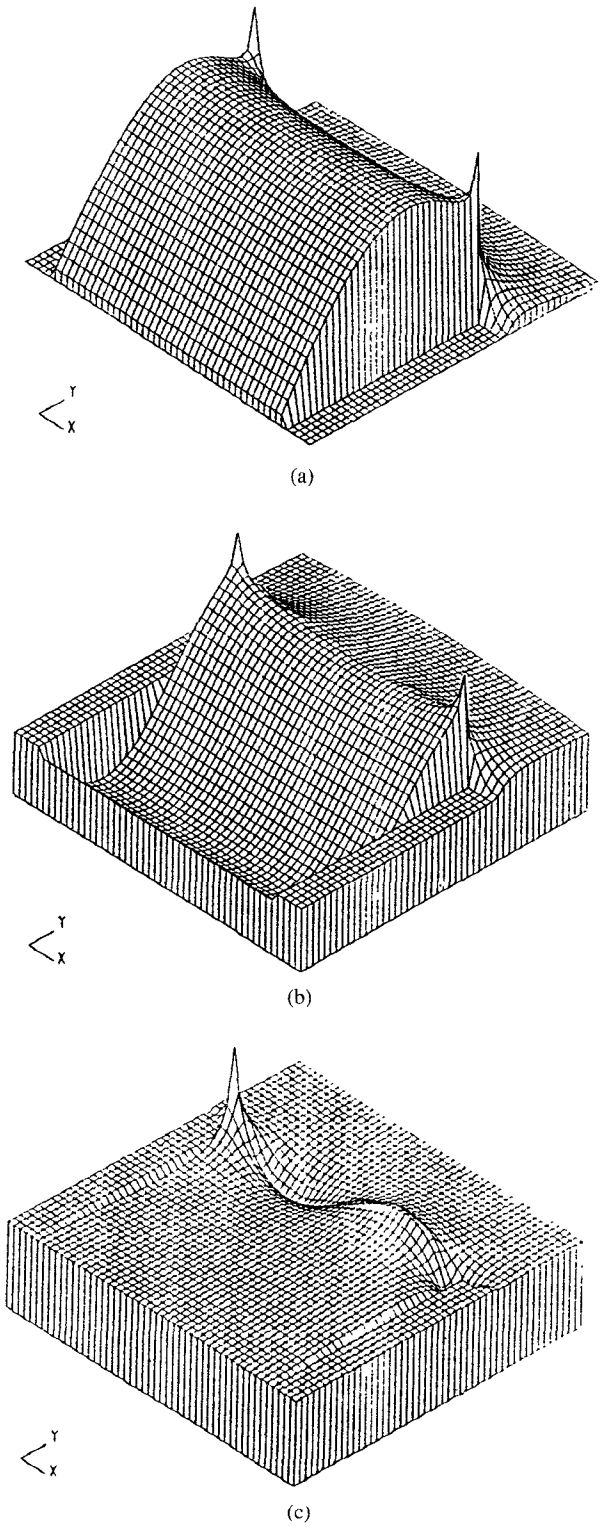

Fig 8. Isometric plot of the E_x field component over the cross section of a single layer PTFE filled IDG of cross section a = 1.016 cm, h = 0.6 cm at 22 GHz Plots shown are for (a) Fundamental (odd) mode, (b) First higher order mode (odd), (c) Second higher order mode (even).

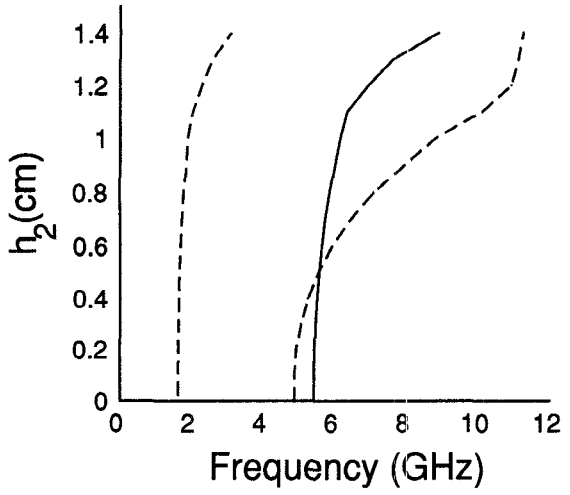

Fig. 9. Variation in cut-off frequencies of the first three modes of two-layer IDG as a function of the thickness of the dielectric layers. The upper layer has $\epsilon_r = 10.2$ while the lower is PTFE. $a = 1.016$ cm, $h = 1.524$ cm.

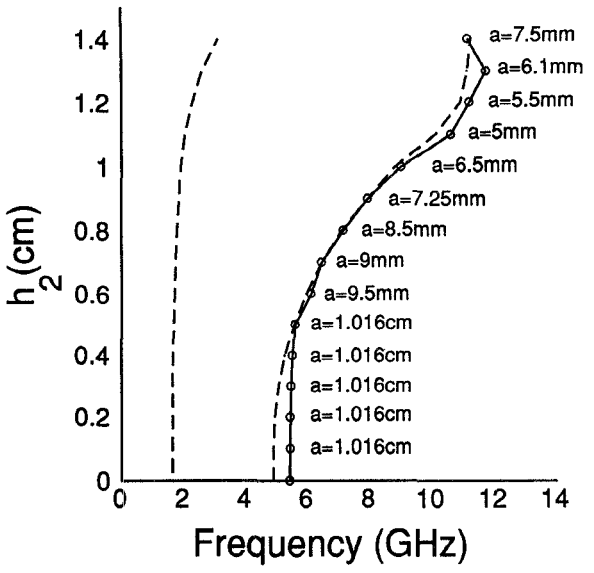

Fig. 10. Variation in cut-off frequency of the first three modes of two-layer IDG as a function of the thickness of the dielectric layers and slot width a. Upper dielectric has $\epsilon_r = 10.2$, lower is PTFE and $h = 1.524$ cm.

V. Bandwidth Control in Multilayered IDG

Consider the case where there are two dielectric layers in the IDG slot. The cutoff frequencies of the first three modes is shown in Fig. 9 as a function of the depth of the top dielectric filling for such a guide. The slot aspect ratio used is 0.67, which is the optimum bandwidth aspect ratio for the single-layered IDG. A relatively high permittivity material ($\epsilon_r = 10.2$) was used for the top dielectric layer. It can be seen that the effect of introducing the higher permittivity layer is to reduce the cutoff frequency of the modes, and, as the thickness of the top layer is increased the cutoff frequencies decreases further as expected. However, whereas the variation of cutoff for the first odd and even modes follows a similar pattern, the cutoff of the second odd mode remains relatively unchanged until the top dielectric layer penetrates significantly into the bulk of the guide. The field patterns given in Fig. 6 may offer an explanation for this behavior since for the second odd mode, a higher order mode pattern is set up within the bulk of the slot, and thus the mode remains unperturbed if a thin dielectric layer is introduced at the top of slot.

With the slot dimensions used so far, using two dielectrics produces no increase in monomode bandwidth over that attainable using only one layer. However, a significant increase in monomode bandwidth is obtained if the width of the slot is controlled in addition to the dielectric filling. This can be seen in Fig. 10 where for a particular dielectric filling, the width of the slot is decreased in order to increase the cutoff of the even mode (as was done for a single-layered IDG).

In Fig. 11 the monomode bandwidth is plotted as a function of dielectric filling for the IDG dimensions of Fig. 10. Clearly, the maximum monomode bandwidth is about 66%, a significant increase over the 50% achieved for the single layered IDG. Fig. 11 thus shows that significant improvement in monomode bandwidth is achievable by choosing an appropriate dielectric filling and cross

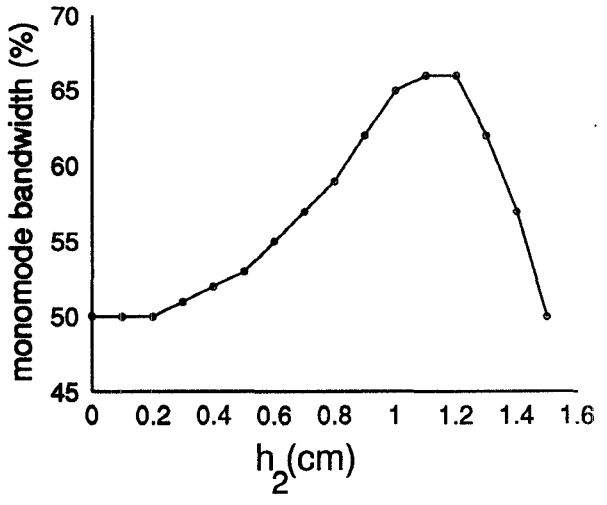

Fig. 11. Optimum bandwidth achievable in two-layer IDG as a function of the thickness of the lower dielectric. Upper dielectric has $\epsilon_r = 10.2$, lower is PTFE and $h = 1.524$ cm.

sectional dimensions for a multilayered IDG. It is also very interesting to note that the dielectric thicknesses can vary over quite a range around its optimum value without affecting the bandwidth much. Hence the guide bandwidth should be quite tolerant to manufacturing variations in the dielectric thicknesses. The dispersion characteristics for the dimensions giving maximum bandwidth in Fig. 11 are presented in Fig. 12, showing a monomode bandwidth between about 2 GHz and 11 GHz.

The cutoff frequencies of the IDG modes scale linearly with guide dimensions, and so a simple comparison with rectangular waveguide and double ridge waveguide can be drawn. A two-layer IDG with an upper cut-off frequency of 42 GHz and a 66% bandwidth has a fundamental cut-off frequency of 8.6 GHz. Such a guide can cover the rectangular waveguide bands WR28 (usual operating range 26.5 GHz–40 GHz and higher order mode propa-

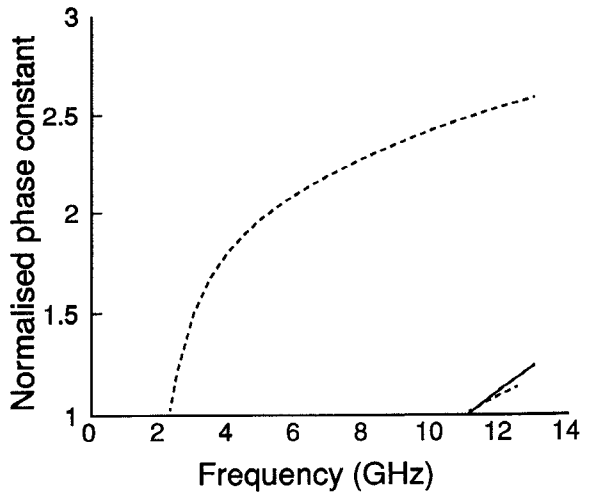

Fig. 12. Dispersion data for two-layer IDG with cross section chosen to give the maximum monomode bandwidth of 66%. a = 5.5 mm, h = 1.524 cm, upper dielectric has ϵ_r = 10.2 and thickness h_1 = 0.324 cm, lower dielectric is PTFE.

gation above 42 GHz), WR42 (18 GHz–26.5 GHz), WR62 (12.4 GHz–18 GHz) and part of WR90 (8.2 GHz–12.4 GHz). The two-layer IDG can cover the double ridge band WRD180-D24 (18 GHz–40 GHz) and part of WRD750-D24 (7.5 GHz–18 GHz).

VI. Conclusions

We have studied Inset Dielectric Guide with a multilayer dielectric filling, using the Transverse Resonance Diffraction technique. Convergence and numeric efficiency of the analysis is good, and comparisons with experimental measurements of phase constant show the validity of the data produced.

We have investigated those aspects of the IDG structure that limit its monomode bandwidth when filled with a single dielectric. It has been shown how the monomode bandwidth of such an IDG may be made greater than that of rectangular metal waveguide by appropriate choice of aspect ratio. Further, we have also shown how the simple use of two dielectric layers in the IDG slot can yield a guide whose monomode bandwidth is 66%, which is much greater than the typical operating bandwidth of standard double ridge waveguide (40%). In the maximum bandwidth configuration, variations in the position of the boundary between the dielectrics produces little change in bandwidth. Hence it appears that multilayer IDG is an attractive transmission media for wideband applications at both microwave and millimeter wave frequencies.

Appendix A
Formulation of Admittance Operators

The tangential magnetic fields at $y = 0^-$ are expressed in terms of the tangential electric fields at $y = 0$ to give [10]:

$$\begin{bmatrix} H_z(x, 0^-) \\ -H_x(x, 0^-) \end{bmatrix} = \begin{bmatrix} \tilde{y}^s_{11} & \tilde{y}^s_{12} \\ \tilde{y}^s_{21} & \tilde{y}^s_{22} \end{bmatrix} \begin{bmatrix} E_x(x, 0) \\ E_z(x, 0) \end{bmatrix} \quad \text{(A1)}$$

where

$$\tilde{y}^s_{11} E_x(x, 0) = \sum_n (\cos^2\theta\, Y_1'^D(n) + \sin^2\theta\, Y_1''^D(n)) \cdot \phi_{hn}(x) \int_0^\infty E_x(x, 0)\phi_{hn}(x)\, dx \quad \text{(A2a)}$$

$$\tilde{Y}^s_{12} E_z(x, 0) = \sum_n j \cos\theta \sin\theta (Y_1'^D(n) - Y_1''^D(n)) \cdot \phi_{hn}(x) \int_0^\infty E_z(x, 0)\phi_{en}(x)\, dx \quad \text{(A2b)}$$

$$\tilde{y}^s_{21} E_x(x, 0) = \sum_n -j \cos\theta \sin\theta (Y_1'^D(n) - Y_1''^D(n)) \cdot \phi_{en}(x) \int_0^\infty E_x(x, 0)\phi_{hn}(x)\, dx \quad \text{(A2c)}$$

$$\tilde{y}^s_{22} E_z(x, 0) = \sum_n (\sin^2\theta\, Y_1'^D(n) + \cos^2\theta\, Y_1''^D(n)) \cdot \phi_{en}(x) \int_0^\infty E_z(x, 0)\phi_{en}(x)\, dx \quad \text{(A2d)}$$

and

$$\cos\theta = \frac{n\pi/a}{\sqrt{(n\pi/a)^2 + \beta^2}} \quad \sin\theta \frac{\beta}{\sqrt{(n\pi/a)^2 + \beta^2}} \quad \text{(A2e)}$$

$Y_1'^D$, $Y_1''^D$ denote the input admittances looking down at interface 1.

Similarly for the air region

$$\begin{bmatrix} -H_z(x, 0^+) \\ H_x(x, 0^+) \end{bmatrix} = \begin{bmatrix} \tilde{y}^a_{11} & \tilde{y}^a_{12} \\ \tilde{y}^a_{21} & \tilde{y}^a_{22} \end{bmatrix} \begin{bmatrix} E_x(x, 0) \\ E_z(x, 0) \end{bmatrix} \quad \text{(A3)}$$

where

$$\tilde{y}^a_{11} E_x(x, 0) = \int_0^\infty (\cos^2\alpha\, Y_1'^U(\rho) + \sin^2\alpha\, Y_1''^U(\rho)) \cdot \phi_h(x, \rho) \int_0^\infty E_x(x, 0)\phi_h(x, \rho)\, dx\, d\rho \quad \text{(A4a)}$$

$$\tilde{y}^a_{12} E_z(x, 0) = \int_0^\infty j \cos\alpha \sin\alpha (Y'(\rho)^U - Y''(\rho)^U) \cdot \phi_h(x, \rho) \int_0^\infty E_z(x, 0)\phi_e(x, \rho)\, dx\, d\rho \quad \text{(A4b)}$$

$$\tilde{y}^a_{12} E_x(x, 0) = \int_0^\infty -j \cos\alpha \sin\alpha (Y_1'^U(\rho) - Y_1''^U(\rho)) \cdot \phi_e(x, \rho) \int_0^\infty E_x(x, 0)\phi_h(x, \rho)\, dx\, d\rho \quad \text{(A4c)}$$

$$\tilde{y}^a_{22} E_z(x, 0) = \int_0^\infty (\sin^2 \alpha Y_1'^U(\rho) + \cos^2 \alpha Y_1''^U(\rho)) \cdot \phi_e(x, \rho) \int_0^\infty E_x(x, 0) \phi_e(x, \rho)\, dx\, d\rho \tag{A4d}$$

and

$$\cos \alpha = \frac{\rho}{\sqrt{\rho^2 + \beta^2}} \quad \sin \alpha \frac{\beta}{\sqrt{\rho^2 + \beta^2}} \tag{A4e}$$

$Y_1'^U$, $Y_1''^U$ denote the input admittances looking up from interface 1.

Applying the boundary conditions on the magnetic fields gives

$$\begin{bmatrix} \tilde{y}_{11} & \tilde{y}_{12} \\ \tilde{y}_{21} & \tilde{y}_{22} \end{bmatrix} \begin{bmatrix} E_x(x, 0) \\ E_z(x, 0) \end{bmatrix} = \underline{0} \tag{A5a}$$

where

$$\tilde{y}_{ii} = \tilde{y}^a_{ii} + \tilde{y}^s_{ii}. \tag{A5b}$$

In order to obtain faster convergence in computing the impedance expressions (A2), (A4), and to be able to use the same set of basis functions for both components of the electric fields, the impedance expressions in (A2) and (A4) can be reformulated in terms of $E_x(x, 0)$, $\partial_x E_z(x, 0)$ as follows. Consider the expressions (A2) for example. Integrating the expressions by parts gives

$$\begin{bmatrix} H_z(x, 0^-) \\ -\int H_x(x, 0^-)\, dx \end{bmatrix} = \begin{bmatrix} \tilde{Y}^s_{11} & \tilde{Y}^s_{12} \\ \tilde{Y}^s_{21} & \tilde{Y}^s_{22} \end{bmatrix} \begin{bmatrix} E_x(x, 0) \\ \partial_x E_z(x, 0) \end{bmatrix} \tag{A6}$$

where

$$\tilde{Y}^s_{11} E_x(x, 0) = \sum_n (\cos^2 \theta\, Y_1'^D(n) + \sin^2 \theta\, Y_1''^D(n)) \cdot \phi_{hn}(x) \int_0^\infty E_x(x, 0)\, \phi_{hn}(x)\, dx \tag{A7a}$$

$$\tilde{Y}^s_{12} \partial_x E_z(x, 0) = \sum_n j \cos \theta \sin \theta (Y_1'^D(n) - Y_1''^D(n)) \cdot \phi_{hn}(x) \frac{a}{n\pi} \int_0^\infty \partial_x E_z(x, 0)\, \phi_{hn}(x)\, dx \tag{A7b}$$

$$\tilde{Y}^s_{21} E_x(x, 0) = \sum_n -j \cos \theta \sin \theta (Y_1'^D(n) - Y_1''^D(n)) \frac{a}{n\pi} \cdot \phi_{hn}(x) \int_0^\infty E_x(x, 0)\, \phi_{hn}(x)\, dx \tag{A7c}$$

$$\tilde{Y}^s_{22} \partial_x E_z(x, 0) = \sum_n (\sin^2 \theta\, Y_1'^D(n) + \cos^2 \theta\, Y_1''^D(n)) \frac{a}{n\pi} \cdot \phi_{hn}(x) \frac{a}{n\pi} \int_0^\infty \partial_x E_z(x, 0)\, \phi_{hn}(x)\, dx. \tag{A7d}$$

Similar expressions can be derived for the air region. Finally by imposing the boundary conditions on the magnetic field components gives

$$\begin{bmatrix} \tilde{Y}_{11} & \tilde{Y}_{12} \\ \tilde{Y}_{21} & \tilde{Y}_{22} \end{bmatrix} \begin{bmatrix} E_x(x, 0) \\ \partial_x E_z(x, 0) \end{bmatrix} = \underline{0} \tag{A8a}$$

where

$$\tilde{Y}_{ii} = \tilde{Y}^a_{ii} + \tilde{Y}^s_{ii}. \tag{A8b}$$

References

[1] S. Hedges and T. Rozzi, "The loss analysis of inset dielectric guide including bending loss and a comparison with image line," Paper P4.5, in *17th European Microwave Conf. Rec.*, Rome, Sept. 1987, pp. 933–938.

[2] T. Rozzi and L. Ma, "Mode completeness, normalization and Green's function of the inset dielectric guide," *IEEE Trans. Microwave Theory Tech.*, vol. 36, pp. 542–551, Mar. 1988.

[3] L. Ma, S. R. Pennock, and T. Rozzi, "Linear arrays realized in IDG," Paper 6, *IEEE Colloquium* "Components for novel transmission lines," Dig. No. 1990/048, London, Mar. 26, 1990.

[4] T. Rozzi and L. Ma, MTT-S 1990, "An efficient mode launcher for array of longitudinal dipoles in IDG," in *IEEE MTT-S. Int. Microwave Symp. Dig.*, Dallas, 1245, May 1990, pp. 1243–1245.

[5] T. Rozzi, S. R. Pennock, and D. Boscovic, "Dispersion characteristics of coupled inset dielectric guides," Paper P1.20, pp. 1175–1180, in *Proc. 20th European Microwave Conf.*, Budapest, Sept. 1990.

[6] J. Kot and T. Rozzi, "Rigorous modeling of single and coupled rectangular waveguide by transverse resonance diffraction," in *Proc. 14th European Microwave Conf.*, Liege, Sept. 1984, pp. 424–429.

[7] C. A. Olley and T. Rozzi, "Characterisation of unilateral finline mode spectrum including loss analysis," in *Proc. 16th European Microwave Conf.*, Dublin, Sept. 1986, pp. 511–516.

[8] S. Hedges and T. E. Rozzi, "The analysis of inset dielectric waveguide using transverse resonance diffraction," in *Proc. 15th European Microwave Conf.*, Paris, Sept. 1985, pp. 743–749.

[9] L. B. Felsen and N. Marcuvitz, *Radiation and Scattering of Waves*. Englewood Cliffs, NJ: Prentice-Hall, 1973.

[10] T. Rozzi and S. Hedges, "Rigorous analysis and network modeling of the inset dielectric guide," *IEEE Trans. Microwave Theory Tech.*, vol. MTT-35, pp. 823–833, Sept. 1987.

[11] I. S. Gradshteyn and I. M. Ryshik, *Tables of Integrals, Series and Products*. New York: Academic Press, 1965.

Steve R. Pennock (M'88) was born in Birmingham, U.K., in 1959. He received the degree of B.Sc in physics with electronics from the University of Liverpool, U.K., in 1980 and the degree of Ph.D from the University of Bath, U.K., in 1986 for his work on the plasmatic control of dielectric waveguides.

From 1983 to 1985 he was a Research Assistant working on Finline Components for Millimetre Waves at the University of Bath, where, in 1985 he became a lecturer. His current research interests include the modeling of novel transmission lines, uniform and nonuniform transmission structures, antennas, active and control circuits, and measurements, at microwave and millimetre wave frequencies.

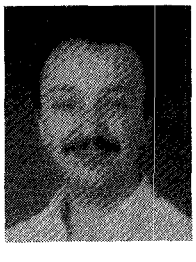

Narian Izzat received the degree of B.Sc in physics with electronics from the University of Southampton in 1984, and in 1986 he was awarded the degree of M.Sc in digital communication from Imperial College in 1988. In 1991 he received the degree of Ph.D from the University of Bath following his research on microstrip and Inset Dielectric Guide structures.

He is currently working as an Assistant Lecturer at the University of Philadelphia. His main research interest is the investigation and analysis of novel waveguide structures.

Tullio Rozzi (M'66–SM'74–F'90), for a photograph and biography, see this issue, p. 1888.